Integrated Optical Proton Exchanged TM-Pass Polarizers in $LiNbO_3$: Modelling and Experimental Performance

Uwe Hempelmann, *Member, IEEE,* Harald Herrmann, Gerd Mrozynski, *Member, IEEE,* Volker Reimann, and Wolfgang Sohler

***Abstract*—Integrated optical TM-pass polarizers operating at wavelengths around $\lambda = 1.5$ μm have been realized by introducing proton exchanged regions adjacent to a Ti-indiffused waveguide on X-cut, Y-propagating lithium niobate. Structural investigations of the proton exchanged regions have been carried out by raster electron microscope and optical methods, in order to characterize the index profile created by the proton exchange. Several polarizers with different geometries of the proton exchanged regions have been analysed numerically by employing the beam propagation method (BPM) and the finite element method (FEM). The device performance is shown to depend strongly on the geometrical shape of the outer boundaries of the proton exchanged regions and on their distance to the channel waveguide. Experimental results are given for several samples with different gaps between the optical waveguide and the proton exchanged regions as well as for different annealing times. For a proper device design a TE-extinction of -26 dB and a TM-excess loss of only 1.2 dB have been obtained experimentally.**

I. Introduction

POLARIZERS are one of the key components in integrated optical circuits and, therefore, several principles of operation have been exploited to develop TM- and TE-pass polarizers. One of those principles takes advantage of the change of anisotropy induced by a proton exchange in $LiNbO_3$. It yields an increase of the extraordinary refractive index and a slight decrease of the ordinary one.

The fabrication of integrated optical polarizers for Ti:$LiNbO_3$ channel waveguides by using an additional proton exchange process has already been reported in [1] for a wavelength of 0.83 μm with 30 dB extinction ratio and 1 dB insertion losses. Many applications, especially for telecommunication systems, require polarizers for the 1.5 μm wavelength range. Therefore, in recent years several authors have applied the same principle of operation to polarizers for this spectral range [2]–[5].

Moreover, the polarizers should be suitable to be integrated into more complex optical circuits. Therefore, especially the fabrication process and the geometrical dimensions of the polarizers must be optimized with respect to this objective. Thereby, several problems have to be solved. In particular, small sizes of the polarizers can result in a low extinction ratio if the geometrical dimensions are not appropriately chosen.

In this paper we present results of a detailed analysis of polarizer structures yielding the critical design parameters and providing guidelines for the optimization of the polarizer structure. In Section II a short description of the operational principle is given. The fabrication process and structural investigations of the proton exchanged regions are described in Section III. In Section IV a theoretical model describing the polarizers is developed allowing a numerical analysis; some examples for various polarizer structures are discussed. Results of the experimental investigations of the polarizers are given in Section V. Finally, the experimental und numerical results are compared and discussed in Section VI.

Manuscript received November 29, 1994; revised April 26, 1995. This work was supported by the Heinz-Nixdorf-Institut of the University of Paderborn and by the European Union within the RACE-project R 2028 'MWTN'.

U. Hempelmann and G. Mrozynski are with Fachgebiet Theoretische Elektrotechnik, Universität-GH Paderborn, 33095 Paderborn, Germany.

H. Herrmann, V. Reimann, and W. Sohler are with Fachgebiet Angewandte Physik, Universität-GH Paderborn, 33095 Paderborn, Germany.

IEEE Log Number 9413043.

II. Principle of Operation

The basic structure of the TM-pass polarizer that can be realized in X-cut $LiNbO_3$ with Y-propagation is depicted in Fig. 1. It consists of two proton exchanged regions adjacent to a Ti-indiffused optical waveguide at both sides.

The proton exchange increases the extraordinary index of refraction, whereas the ordinary index is decreased [1]. Therefore, the extraordinary polarized optical waves (TE) are coupled into the proton exchanged regions as indicated by the arrows in Fig. 1. For the ordinary polarization (TM) the field remains localized in the Ti-diffused channel waveguide, which has the highest index of refraction.

Considering the crystal orientation mentioned above, the device operates as a TM-pass polarizer. In Z-cut $LiNbO_3$ the same structure gives a TE-pass polarizer.

To allow the integration of such polarizers with other optical devices, sufficiently small dimensions, as well in length as in width, are required. A reduction of the width can result in a coupling back of TE-waves into the optical waveguide after a reflection at the outer boundaries of the proton exchanged regions. Therefore, the shape of the outer boundaries determines strongly the extinction properties of the polarizers. As will be outlined in the subsequent sections, zig-zag shaped outer boundaries—as already indicated in Fig. 1—are suitable to suppress these reflections. The polarizer length can be reduced by narrowing the gap between the

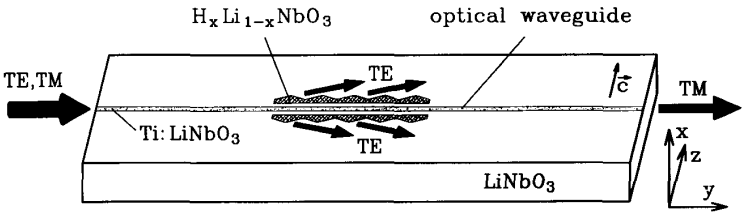

Fig. 1. Structure of the TM-pass polarizer.

two proton exchanged regions, which leads to a stronger coupling for the TE-field, but also causes a greater distortion of the fundamental TM-mode and—as a consequence—a larger excess loss.

III. Fabrication of Polarizers and Characterization of PE:$LiNbO_3$

A. Fabrication

By indiffusion of 1050 Å thick, 7 μm wide Ti stripes (1020°C, 9 h) monomode (λ =1.55 μm) optical waveguides of low propagation losses (< 0.2 dB/cm) have been fabricated in X-cut Y-propagation $LiNbO_3$ first.

Then a vacuum-evaporated metallic mask has been deposited on the substrate with openings for the subsequent proton exchange yielding the polarizers. It proved to be very important to have a tight exchange mask without any pinholes to avoid excess propagation losses caused from scattering by inhomogeneities due to unwanted proton exchange through such holes. After studying several materials and evaporation parameters to fabricate the exchange mask the following process has been found that guarantees the required tightness: First a 1500 Å thick titanium layer is deposited on the surface. During the evaporation process two about 100 Å thick intermediate layers of titaniumdioxide are formed by increasing the oxygene partial pressure in the evaporation chamber. Then a photoresist is spin-coated on the Ti/TiO_2-layer; the areas for the subsequent proton exchange are defined by a photolithographic process and opened by wet etching, using a mixture of 1% HF and 1% HNO_3. Afterwards, the sample is covered in the range of the polarizers by a metal foil and coated again with an additional 1500 Å thick titanium layer (here without TiO_2 intermediate layers) to improve the protective coating on top of the waveguide.

The proton exchange is performed at 250°C in an evacuated closed quartz tube during 15.5 h. As proton source benzoic acid diluted with 1 mol% lithium benzoate is used. After the proton exchange and the removal of the exchange mask the sample is annealed at T_a = 330°C in an O_2 atmosphere for at least 2 hours. This step proved to be necessary to compensate the oxygen loss at the crystal surface caused by oxydation under the Ti mask. Furthermore, the annealing process results in a proton diffusion. Therefore, the polarizer performance can be adjusted after the proton exchange by using the annealing time t_a as free parameter.

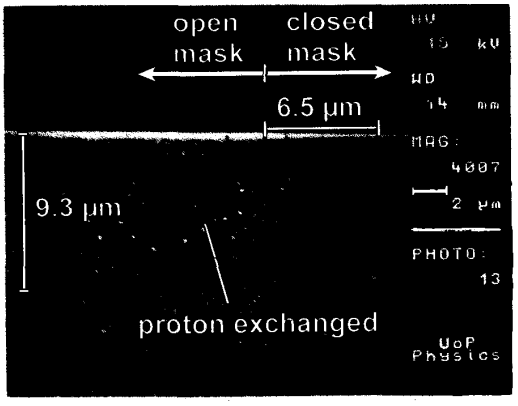

Fig. 2. Micrograph of a cross section of an etched proton exchanged layer taken by a raster electron microscope. The boundary of the former exchange mask is sketched in the micrograph. The exchange depths are d_{Ex} = 6.5 μm and d_{Ez} = 9.3 μm, respectively. (The dark line nearly parallel to the surface is due to a scratch on the sample.)

B. Structural Investigations

For the numerical modelling of the polarizers (see Section IV) an accurate knowledge of the index profile is necessary. Therefore, several experiments have been performed to characterize the index profile with regard to the depths of the proton exchange d_{Ex} and d_{Ez} and the index change $\delta n_{e,E}$ and $\delta n_{o,E}$.

Preferential Etching and REM-Investigations: To get an impression of the depth of the proton exchange, the first experiment was to prepare an X-cut sample with a wide proton exchanged area and large exchange depth. The sample has been exchanged for 90.5 h at a temperature of 270°C using benzoic acid diluted with 1 mol% lithium benzoate. Afterwards—without any annealing—it has been cut and polished perpendicular to the Y-axis, before it has been put in a mixture of 3 molar HF and HNO_3 each. Proton exchanged $LiNbO_3$ etches along the Y-axis much faster than pure $LiNbO_3$, as reported in [6]. Therefore, a proton exchanged layer can be seen as a step, if the X-cut crystal is polished perpendicular to the Y-axis and afterwards etched. The micrograph in Fig. 2, taken by a raster electron microscope (REM), shows such a cross section of a $LiNbO_3$-crystal with an etched proton-exchanged area. The step between the pure and the exchanged area proved to be very sharp. One reason is that the profile of the proton concentration is nearly step-like, as reported in [7], [8]. Another reason may be that the etching velocity abruptly decreases at a fixed proton concentration. The evaluation of such micrographs yields an exchange depth

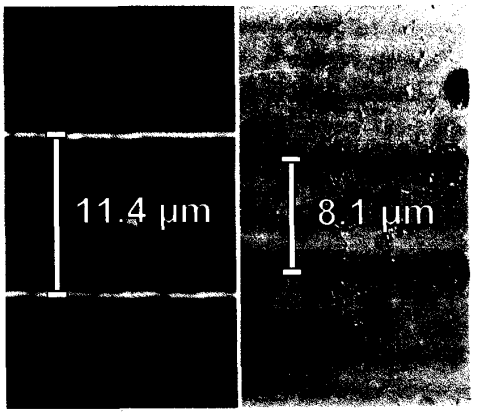

Fig. 3. Photographs of a polarizer segment (a) before and (b) after the removal of the exchange mask. Left: The photograph shows the Ti-TiO_2 stripe-like mask of 11.4 μm width to prevent proton exchange in the optical waveguide region. Right: After the proton exchange and removal of the mask taken photograph revealing the proton exchange boundaries as dark lines. From them the figure of the side-diffusion in Z-direction is d_{Ez} = (11.4 μm −8.1 μm)/2 =1.65 μm (see also text).

of d_{Ex} = 9.3 μm. Furthermore, the lateral etch width in Z-direction proved to be d_{Ez} = 6.5 μm larger than the actual mask opening, which is attributed to side diffusion.

To get information on the exchange depth d_{Ex} of the actual polarizers, several polarizer-samples have been cut, polished and etched for investigations with the REM yielding an exchange depth of d_{Ex} = 2.5 μm with an accuracy of about 0.5 μm.

Optical Microscope Investigations: To analyze the side diffusion the polarizers have been investigated using an optical microscope with the diffential interference contrast method. In Fig. 3 photographs before the proton exchange (left) and after the exchange (right) are shown. In the left photograph the boundaries of the stripe-like Ti/TiO_2 exchange mask covering the optical waveguide are visible as white lines separated by 11.4 μm. After the exchange and after the removal of the mask the borders of the proton exchanged areas can be seen as dark lines in Fig. 3 (right) separated by 8.1 μm. From this result we deduced a side diffusion depth of d_{Ez} = 1.65 μm.

As the proton exchange changes the birefringence $\Delta n = n_e - n_o$ of $LiNbO_3$, the integrated polarizer can be studied using polarized light. The simplest approach is to illuminate the sample under microscopic control with monochromatic light linearly polarized under 45° with respect to the crystal axes Y and Z and to observe the polarizer through an analyzer under +45° or −45°. As the state of polarization (SOP) of the light after traversing the sample will in general be elliptical depending on the birefringence of the material transmitted, the shape of the proton exchanged structure can be clearly seen. Moreover, the polarizing microscope allows an even more detailed analysis of the proton exchanged structure, if an additional wedge fabricated of X- or Y-cut $LiNbO_3$ is used. Such a wedge of about 2° angle has been positioned on the surface of the sample using some immersion oil with the c-axes of the wedge and sample being parallel (see Fig. 4). In that way bright and dark fringes have been observed on the

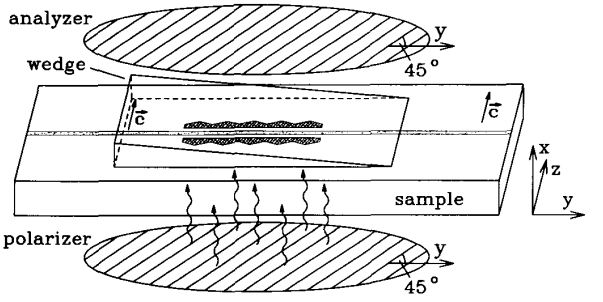

Fig. 4. Experimental setup for microscopic investigations.

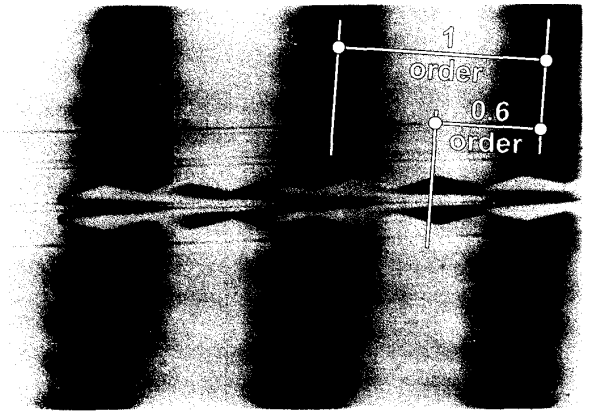

Fig. 5. Photograph of a fringe pattern obtained with the set-up sketched in Fig. 4. At λ = 589 nm a fringe shift above the integrated polarizers of α^{589} = 0.6 order has been obtained.

surface of the wedge perpendicular to the optical waveguide, as loci of a linear SOP. Due to the different birefringence of proton exchanged material and unmodified $LiNbO_3$ these fringes are shifted above the integrated polarizers towards the $+Y$-direction (see Fig. 5). To be specific, for the polarizers to be discussed in Section V a shift of 0.6 orders has been observed in the visible at λ = 589 nm (α^{589} = 0.6). Analyzing this fringe shift we obtain

$$\alpha = \frac{1}{\lambda}\int_0^{-D} [\Delta n_{e,E}(x) - \Delta n_{o,E}(x)]\, dx \qquad (1)$$

where $\Delta n_{i,E}(x) = \delta n_{i,E} \cdot g_i(x)$ $(i = e, o)$ are the index variations caused by the proton exchange and D is a sufficiently large depth with $\Delta n_{i,E}(D) = 0$. $g_i(x)$ are the shape functions of the ordinary and extraordinary index profiles. Assuming step-like index profiles with the same depth, i.e. $g_e(x) \equiv g_o(x)$ for unannealed samples [7], [8] (1) simplifies to

$$\alpha = \frac{d_{Ex}}{\lambda}[\delta n_{e,E} - \delta n_{o,E}] \qquad (2)$$

where d_{Ex} is the depth of the proton exchange. Using (2) the exchange depth d_{Ex} can now be determined via the measured fringe shift, if both index changes $\delta n_{e,E}$ and $\delta n_{o,E}$ are known.

In order to find these two figures, the unannealed X-cut sample mentioned above with a wide proton exchanged area and large exchange depth, has been investigated. Due to

the sligthly unparallel surfaces a Fizeau type interferometer is formed, its fringes have been analysed using polarized light ($\lambda = 1545$ nm). By passing from proton exchanged to unexchanged regions, abrupts shifts in the stripe pattern occur which are related to the exchange depth and index change by

$$\beta_i = 2\frac{d_{Ex}}{\lambda}\delta n_{i,E} \qquad (i = e, o). \tag{3}$$

The shifts have been measured to be $\beta_e = 1.2$ and $\beta_o = -0.3$, respectively. By the preferential etching experiments an exchange depth of $d_{Ex} = 9.3$ μm has been determined. With (3) and d_{Ex} the index changes $\delta n_{i,E}$ at $\lambda = 1545$ nm have been calculated to be $\delta n_{e,E} = 0.10$ and $\delta n_{o,E} = -0.025$ resulting in a birefringence in the proton exchanged area of $\delta n_{e,E} - \delta n_{o,E} = 0.125$.

The microscope experiment with the wedge at $\lambda = 589$ nm also has been performed with this deeply exchanged sample. Applying (2) to the measured fringe shift of $\alpha^{589} = 2.25$ the difference in the index changes have been calculated to $\delta n_{e,E} - \delta n_{o,E} = 0.1425$. With this figure, (2) and $\alpha^{589} = 0.6$ and the approximation of a step-like index profile the exchange depth of the polarizers has been determined to be $d_{Ex} = 2.47$ μm, which agrees very well with the results described in Section III-B-1.

This optical method has the advantage to be non-destructive. The depth of the proton exchange can be easily checked by an examination of the integrated polarizers with the birefringent wedge using a polarizing microscope.

IV. Numerical Analysis

In order to get detailed information on the optical wave propagation in the polarizer, numerical calculations have been carried out by using the refractive index model described below. For the crystal orientation given here, the dielectrical tensor is diagonal and hence no coupling between the (quasi-)transverse electric (TE) and the (quasi-)transverse magnetic (TM) field occurs. Therefore, the two polarizations can be analysed separately by using the modified Helmholtz equation in the scalar approximation [9]

$$\left[\alpha_x^2\frac{\partial^2}{\partial x^2} + \alpha_z^2\frac{\partial^2}{\partial z^2} + \frac{\partial^2}{\partial y^2} + k_0^2 \cdot n_i^2(x,y,z)\right]\Psi = 0. \tag{4}$$

In this equation the function $n_i(x, y, z)$ denotes the index of refraction and k_0 is the vacuum propagation constant. The subscript $i = o, e$ has been introduced to distinguish between the ordinary and extraordinary index. As indicated in Fig. 1, the orientation of the coordinate system (x, y, z) has been taken to be identical to the orientation of the corresponding crystal axes (X, Y, Z). The scalar function Ψ is proportional to one transverse field component and the factors α_x and α_z are quotients of refractive indices. Considering X-cut $LiNbO_3$ with Y-propagating waves, these quantities have to be assigned as follows [10]:

$$\begin{array}{lllll} \text{TE:} & \Psi \propto E_z & n_i = n_e & \alpha_x = 1 & \alpha_z = n_e/n_o \\ \text{TM:} & \Psi \propto H_z & n_i = n_o & \alpha_x = \alpha_z = 1 & \end{array}. \tag{5}$$

Two methods, the three-dimensional beam propagation method (BPM) [11] and the finite element method (FEM) [10], [12], have been used to analyse the performance of the polarizer. The BPM, as a mode independent method, allows the calculation of the total field and is therefore suitable to evaluate the attenuation properties of our device. On the other hand with the FEM a precise calculation of waveguide modes is possible, which has been found to be useful for the explanation of excess TM-losses.

TABLE I
Meanings and Values of Symbols for the Ti- Indiffused Waveguide

Symbol	Meaning	Values
τ	Ti stripe thickness before indiffusion	0.09 μm
W	Ti stripe width before indiffusion	7 μm
D_x	diffusion length in x-direction	3.163μm
D_z	diffusion length in z-direction	3.753μm
d	constant	$1.57{\cdot}10^{-23}$cm^3
$c_0 = \tau/(dD_x)$	maximum Ti concentration for $W \to \infty$	$1.812{\cdot}10^{21}$cm^{-3}
E	constant	$1.2 \cdot 10^{-23}$cm^3
F	constant	$1.3 \cdot 10^{-25}$cm^3
γ	constant	0.55
λ	wavelength	1.52μm
d_e	extraordinary dispersion coefficient	0.8631
d_o	ordinary dispersion coefficient	0.7099
n_{es}	extraordinary substrate index	2.13828
n_{os}	ordinary substrate index	2.21387

A. Model for the Index Change

The mathematical model for the index of refraction is taken to be of the common form

$$n_i(x,y,z) = \begin{cases} n_{i,S} + \Delta n_{i,I}(x,y,z) + \Delta n_{i,E}(x,y,z) & x \le 0 \\ 1 & x > 0 \end{cases} \quad i = o, e\,, \tag{6}$$

where $n_{i,S}$ is the constant substrate index and $\Delta n_{i,I}$, $\Delta n_{i,E}$ denote the index variations caused by the titanium indiffusion and proton exchange, respectively. The local index increase for the Ti-indiffused waveguide $\Delta n_{i,I}$ is described by [10] and [13]

$$\begin{aligned} \Delta n_{eI}(x,z) &= d_e\ Ec(x,z) \\ \Delta n_{oI}(x,z) &= d_o\big[Fc(x,z)\big]^\gamma, \end{aligned} \tag{7}$$

with the local Ti concentration

$$c(x,z) = \frac{c_0}{2}\left[\operatorname{erf}\left(\frac{W-2z}{2D_z}\right) + \operatorname{erf}\left(\frac{W+2z}{2D_z}\right)\right] \times \exp\left(-\frac{x^2}{D_x^2}\right). \tag{8}$$

The meanings and the actual values of the various symbols are given in Table I. It should be noted, that the Ti-stripe thickness taken for the calculations differs from the experimental one ($\tau = 0.105$ μm). The variation of this parameter has been used to match the intensity distribution of measured modal fields which had full widths at half maximum of 6.3 μm (4.5 μm) in horizontal and 3.9 μm (2.7 μm) in vertical directions for TM (TE) polarized optical fields.

As outlined in [7] the annealing process for a proton exchange profile with given exchange depth d_E can be described

TABLE II
MEANINGS AND VALUES OF SYMBOLS FOR THE PROTON EXCHANGED REGIONS

Symbol	Meaning	Values
t_a	annealing time	3.5h
T_a	annealing temperature	330 °C
$\delta n_{e,E}$	extraordinary index difference before annealing	0.1
$\delta n_{o,E}$	ordinary index difference before annealing	−0.025
d_{Ex}	exchange depth in x-direction	2.5μm
d_{Ez}	exchange depth in z-direction	1.65μm
g	gap of the exchange mask	10.7μm
D_a	annealing diffusion coefficient as given in [7]	$2.65{\cdot}10^{11} \cdot e^{-(1.67{\cdot}10^4 K/T_a)\frac{\mu m^2}{h}}$

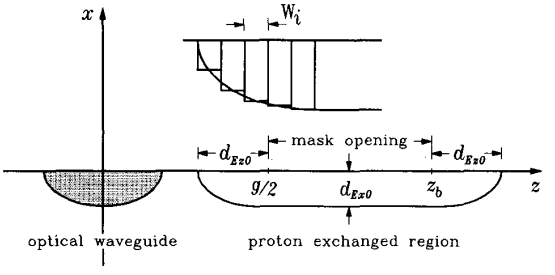

Fig. 6 Sketch of the proton exchange profile before annealing.

by the diffusion process from a source of finite thickness. The model given in [7] includes the diffusion perpendicular to the surface only, since planar structures had been investigated. In TM-pass polarizers the proton exchanged areas are of finite width and especially the index changes close to the Ti-indiffused waveguides are very important for the device performance. That means, we have to describe the index distribution by a two-dimensional function taking into account the lateral proton exchange under the mask opening and even lateral diffusion due to annealing. In [14] a model for the index profile of proton exchanged and annealed channel waveguides has been developed. The authors assumed a rectangular cross section of the proton exchange as starting condition for the annealing process. However, as described in the previous section, we found that the shape of the cross section differs significantly from a rectangular shape as shown in Fig. 2. Therefore, the model given in [14] is not directly applicable to our polarizers.

With respect to the experimentally obtained index profile of the proton exchange, as shown in Fig. 2, the refractive index distribution before annealing is modelled by the profile sketched in Fig. 6. The cross section of the proton exchanged area consists of three sections. Directly under the mask opening the depth of the proton exchange is d_{Ex0}. The side exchange under the mask can be approximated by an ellipse with principal axes $2d_{Ex0}$ and $2d_{Ez0}$, respectively.

Annealing can be described by a diffusion process [7]. To take into account our special proton exchange profile, it is approximated by a finite number of rectangular regions, where the central part is kept unchanged and the elliptical areas are equidistantly decomposed into $l_{\max}$ small rectangular segments, as depicted in the inset of Fig. 6. For the numerical calculations discussed below, a segmentation with $l_{\max} = 5$ proved to be sufficient to describe the index distribution at the boundaries.

The complete refractive index distribution after annealing is then given by summation over all contributions from the rectangular areas

$$\Delta n_{i,E}(x,y,z) = \delta n_{i,E} \cdot \sum_{l=-2l_{\max}-1}^{2l_{\max}+1} f_l(z, z_l, W_{zl}) \cdot g_l(x, W_{xl}) \quad (9)$$

where $\delta n_{i,E}$ denotes the index difference before annealing, which is assumed to be identical in all segments. The diffusion process in both directions for each segment with the center position z_l, with $z_{-l} = -z_l$, is described by the erf-profiles

$$g_l(x, W_{xl}) = \frac{1}{2}\left[\mathrm{erf}\left(\frac{W_{xl} - 2x}{2d_{ax}}\right) + \mathrm{erf}\left(\frac{W_{xl} + 2x}{2d_{ax}}\right)\right]$$

$$f_l(z, z_l, W_{zl}) = \frac{1}{2}\left[\mathrm{erf}\left(\frac{W_{zl} - 2(z - z_l)}{2d_{az}}\right) + \mathrm{erf}\left(\frac{W_{zl} + 2(z - z_l)}{2d_{az}}\right)\right]. \quad (10)$$

The source width in z-direction is $W_{z(l_{\max}+1)} = W_{z(-l_{\max}-1)} = z_b(y) - g/2$ for the rectangular areas and $W_{zl} = W_{z(-l)} = d_{Ez0}/l_{\max}$ for the ellipse. The source width in x-direction is $W_{xl} = 2d_{Ex0}$ for rectangular areas and $W_{xl} = W_{x(-l)} = 2d_{Ex0}\sqrt{1 - (\frac{z_l - z'}{d_{Ez0}})^2}$ for the ellipse. z' is the center position of the respective ellipse, which is $z' = \pm g/2$ for the inner boundaries and $z' = \pm z_b(y)$ for the outer boundaries. The annealing diffusion depths in x- and z-direction are evaluated by the relations [7]

$$d_{ax} = 2\sqrt{D_a t_a}$$
$$d_{az} = 2\sqrt{0.7 D_a t_a}. \quad (11)$$

The meanings of the symbols occuring in (9)–(11) and their values used for the following numerical examples are given in Table II.

B. Extinction of the TE-Polarized Field

First we focus on the BPM-calculations concerning the TE-field beginning with the rectangular polarizer version [1] depicted as underlaid contour in Fig. 8. In what follows all field distributions are represented as $|\Psi|$ and the power has been calculated by the normalized overlap integral of the local field $\Psi(y)$ and the fundamental mode of the Ti:$LiNbO_3$-waveguide Ψ_{00} derived by FEM-calculations. As shown in Fig. 7 at the beginning of the polarizer the TE-fundamental mode (TE_{00}) is almost completely coupled into the adjacent

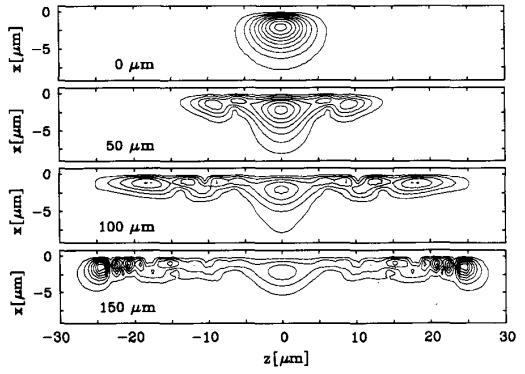

Fig. 7. Evolution of the TE-field, $|E_z|$, at the distances 0, 50, 100, and 150 μm from the beginning of the polarizer (a–d).The fields are normalized to the maximum of theTE_{00}-mode and the isolines are given in 10% steps with the lowest level at 10%.

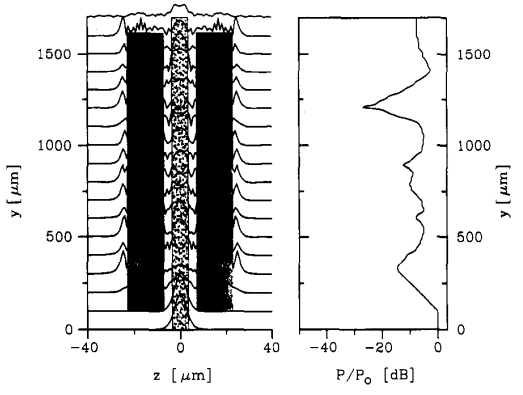

Fig. 8. Power in the TE_{00}-mode and TE-field distribution in the rectangular shaped polarizer. $|E_z|(z, y)$ at $x = -2.1$ μm, $z_b(y) = 22.35$ μm, $L = 1520$ μm.

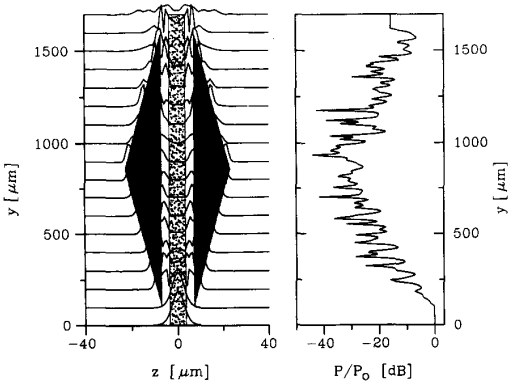

Fig. 9. Power in the TE_{00}-mode and TE-field distribution in the triangular shaped polarizer. $|E_z|(z, y)$ at $x = -2.1$ μm, $g/2 \leq z_b(y) \leq 22.35$ μm, $L = 1520$ μm.

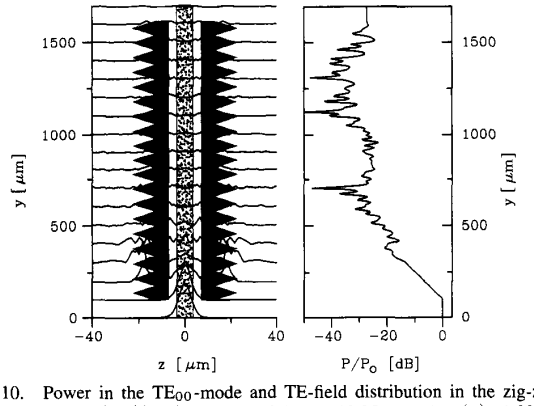

Fig. 10. Power in the TE_{00}-mode and TE-field distribution in the zig-zag shaped polarizer. $|E_z|(z, y)$ at $x = -2.1$ μm, 12.35 μm $\leq z_b(y) \leq 22.35$ μm, $L = 1520$ μm and the period of the outer boundary variation is 80 μm.

strongly guiding proton exchanged regions and only a small amount of the power is initially lost to substrate radiation modes. The field distribution throughout the whole device for the fixed depth $x = -2.1$ μm (localization of the TE_{00}-maximum) is shown in Fig. 8. The polarizer is located between $y = 100$ μm and $y = 1620$ μm.

Being strongly disturbed by the polarizer, the TE-field spreads out into the adjacent proton exchanged regions. At the outer boundaries it is reflected and hence propagates back to the Ti-indiffused waveguide. If the reflected wave is phase matched to the TE_{00}-mode, its power is coupled back into the waveguide as can be seen at about $y = 500$, 1000, and 1400 μm. This coupling is a significant drawback, because thereby the attenuation depends strongly on the device dimensions.

Since the polarizer discussed is homogeneous with respect to the propagation direction, it can be regarded as a waveguiding structure in total. For the TE-field this super-waveguide is strongly guiding and, therefore, a lot of supermodes are excited by the incoming TE_{00}-mode. In this representation the y-dependence of the power guided by the TE_{00}-mode can be explained by the supermode interference. Since the power guided in each supermode is conserved, there is no overall radiation loss with respect to the super-waveguide, except the transition loss at the beginning. In order to obtain a high extinction of the TE-polarized field, the end of the polarizer has to be a plane of destructive interference and, thereby, the optimum device length is a function of all parameters.

To overcome this difficulty the outer boundaries should be modified in such a way that a destructive interference in the channel waveguide is obtained throughout the whole length or that the supermodes are coupled to radiation modes. In view of this goal we have investigated the two modified polarizer versions shown by the underlaid structures in Fig. 9 and 10. The inclinations of the outer boundaries with respect to the y-axis have been determined by the aid of a simple ray optical approximation. The angles of the triangular shaped proton exchanged areas have been chosen to prevent a phase matched coupling of the reflected wave into the central channel waveguide. In the case of the zig-zag shaped boundaries total reflections are avoided, which is equivalent to a coupling of the supermodes to radiation modes. In order to prove these ray optical approximations, BPM calculations have been carried out for both types of polarizers.

For the triangular shaped version it can be seen in Fig. 9 that the field is again confined with respect to the total structure, but in the interval 620 μm $\leq y \leq$ 1000 μm a sufficiently high attenuation is achieved. For $y > 900$ μm the

attenuation decreases again and due to the strong dependence on the propagation distance it would be even less than that of the unmodified polarizer, if its device length is reduced about 50 μm.

These differences to the ray optical approximation which considers only one special geometrical path, is understandable by regarding the local supermodes of the total waveguide structure. As the width continuously increases in the first half of the polarizer, the following three effects have to be taken into account: Starting with TE_{00}, the number of guided modes increases with the width; existing modes are continuously changed with respect to their transverse field distributions and phase constants; all these modes are coupled to each other due to the waveguide variation with respect to the y-coordinate. In the second half the number of guided modes decreases again until only TE_{00} is left and thereby higher order modes are coupled to radiation modes. Hence the power remaining in the fundamental mode depends on the described interaction which itself is determined by the boundary inclination. Considering these complex relations, it will obviously be difficult to find device dimensions suitable to cause a high attenuation. On the other hand the polarizer is well designed, if it consists only of the first part. In this case the field will radiate into the substrate at the end of the polarizer. This is very similar to the polarizer version proposed in connection with the TE/TM-splitter reported in [15].

For the zig-zag shaped version the BPM-calculated field distribution is shown in Fig. 10. In this case the field experiences a continuous coupling to radiation modes at the outer boundaries. Since the TE-polarized field is mainly radiated out of the polarizer when it reaches the boundaries, supermode interference does no longer influence the TE-extinction. Therefore, the attenuation of this polarizer type is not sensitive to the device dimensions. This structure should preferably be used in comparison to the two geometries analysed before to realize polarizers with high extinction ratios.

Since possible numerical errors of the BPM-algorithm are in the order of -50 dB, this inaccuracy has to be considered for power levels below -40 dB. Hence the power values at the minima occuring in Fig. 10 are subject to this uncertainty, but an extinction of 40 dB can be ensured.

C. Evolution of the Transmitted TM-Polarized Field

Besides the above discussed properties concerning the TE-polarization, the device has also been analysed with respect to its influence on the TM-field. Since the ordinary index of refraction is decreased by the proton exchange, the TM_{00}-mode is effected by the polarizer as well.

The results of the BPM-calculations for the zig-zag shaped polarizer are shown in Fig. 11. As can be seen from the normalized power, $\approx$0.67 dB of the guided power is lost on the first 100 μm due to mode mismatch at the beginning of the polarizer. Additionally to this transition loss, the TM_{00}-guided power decreases throughout the whole device length and 1.2 dB are lost at the end (y =1620 μm).

The reason for this high excess loss can be found by a more detailed inspection of the field in the polarizer, as shown in

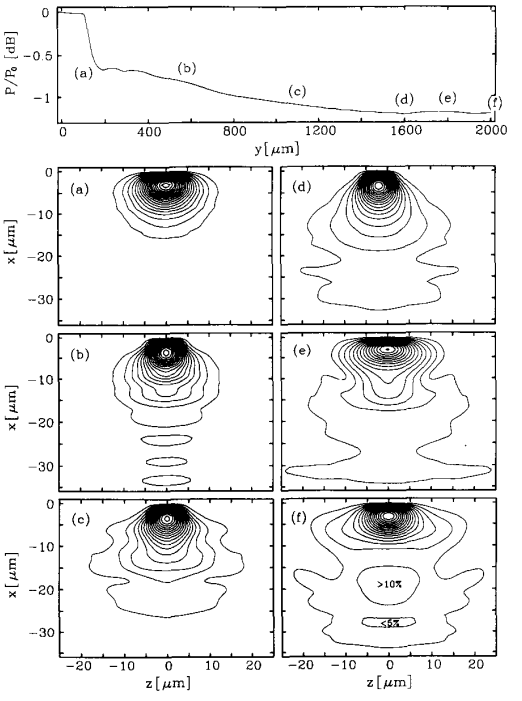

Fig. 11. Power in the TM_{00}-mode and the evolution of theTM-field, $|H_z|$. The polarizer is located at 100 μm $\leq y \leq$ 1620 μm. The fields are normalised to the maximum of the TM_{00}-mode and the isolines are given in 5% steps with the lowest level at 5%.

Fig. 11. Being excited by the TM_{00}-mode of the undisturbed Ti-indiffused waveguide (a), the field in the polarizer becomes more confined between the proton exchanged areas, but it continuously broadens below, (b)–(d). Behind the polarizer those parts of the field that do not overlap with the fundamental mode of the undisturbed waveguide radiate into the substrate, (e), (f). Due to normalization of the fields to the maximum of the TM_{00}-mode, the power loss can also be seen from the disappearance of higher level isolines for increasing propagation distances. Since the narrowing near the proton exchanged areas prevents the field from extending to the outer boundaries, the field distribution and the power are identical for the three polarizer types.

Regarding again the whole structure as one super-waveguide, it also should have a TM_{00}-mode which is different from the fundamental mode of the undisturbed Ti-indiffused channel waveguide. This difference leads to a mode mismatch and is therefore the reason of the high transition loss at the beginning of the polarizer. If the TM_{00}-supermode is guided, a stationary transversal field distribution, and thereby a constant power should be reached asymptotically after a certain propagation distance. For this reason BPM calculations have been performed assuming a device length of 3 cm. But for the data given in Table II no constant power level has been obtained even after this long propagation length. Hence we concluded that the polarizer under consideration does not guide the TM_{00}-supermode.

In order to confirm this assumption, we calculated the lowest order supermode by employing the FEM. In Fig. 12

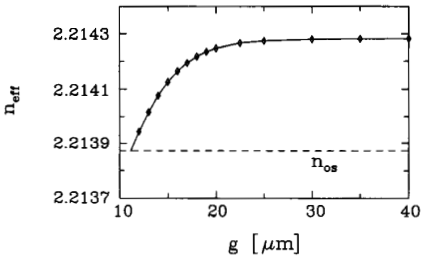

Fig. 12. Calculated effective indices of the TM_{00}-supermode as function of the gap. The dashed line shows the substrate extraordinary refractive index.

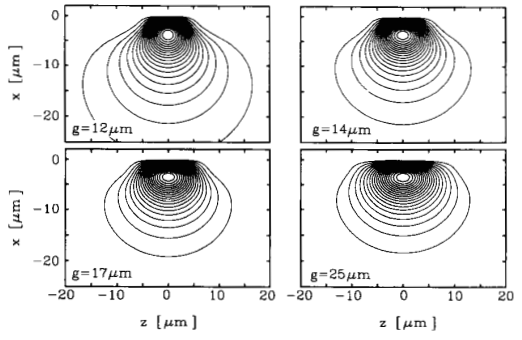

Fig. 13. Topographic view of field distributions of TM_{00}-supermodes for several gaps calculated using the FEM. The isolines belong to field levels between 5% and 95% in 5% steps.

the effective mode index is plotted as a function of the gap between the two opposite proton exchanged regions. For gaps larger than $g = 20$ μm the effective index is only slightly effected by the proton exchanged regions, but for gaps smaller than $g = 20$ μm the effective index decreases strongly. The TM_{00}-supermode is below cutoff for gaps smaller than $g = 11$ μm.

In Fig. 13 the modal fields for several gaps are shown. They are narrowed between the proton exchanged regions, but they are less confined with respect to the vertical direction. In total this effect causes the guidance to decrease and below a certain gap size the TM_{00}-mode is no longer guided. The proton exchange causes a reduction of the effective width and, therefore, a shift below cutoff for small gaps. Since the two different numerical methods lead to the same results, the calculated attenuation of the TM_{00}-mode is due to the weaker guiding of the TM-field and not caused by artificial effects of the BPM-algorithm.

V. Polarizer Performance

The performance of polarizers of the three different versions already discussed in the modelling section has been experimentally investigated at wavelengths around $\lambda = 1500$ nm. TM-excess loss and the TE-extinction loss have been measured as function of the gap width and of the annealing time. Furthermore, we have characterized the temperature dependence of the polarizer performance up to 60°C.

First experiments have been carried out using polarizers with rectangular shaped proton exchanged areas. In Fig. 14 a typical example of the temperature dependence of the TE-extinction is shown. It varies from only 2 dB at 24°C to 13 dB at 39°C resulting in an extreme temperature dependence. The reason for this behaviour can be described as follows: As discussed before, at the beginning of the polarizer the wave is almost completely coupled to the supermodes of the super waveguide. By varying the temperature the optical path length within the polarizer is tuned resulting in a variation of the relative phase differences between the supermodes. Therefore, the interference pattern at the end of the polarizer is temperature dependent and hence also the excitation of the fundamental mode of the strip waveguide leading to the observed temperature dependence of the polarizer performance. This temperature dependence proves the extreme sensitivity to phase variations in the polarizer. Therefore, one can conclude, that the polarizer performance strongly depends on parameters causing similar phase effects, such as geometrical or wavelength variations.

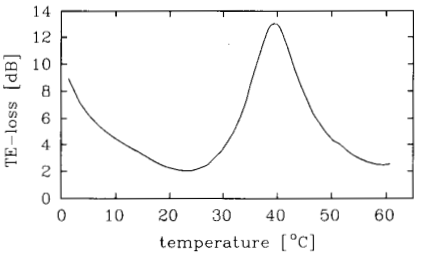

Fig. 14. Measured excess TE loss of a rectangular shaped polarizer versus sample temperature—a typical example.

In accordance with the numerical results a similar behaviour has been obtained for the polarizers of the triangular version resulting again in only small extinction loss.

Several 1.5 mm long TM-pass polarizers with zig-zag shaped outer boundaries, as shown in detail in Fig. 15, have been investigated. The distances between the proton exchanged regions g were 10.7, 11.4 and 12.4 μm, where g refers to the actual exchange mask openings; for each g there exist 6 polarizers. To study the dependence of the polarizer performance on the annealing time, the samples have been annealed 3 times at 330°C leading to total annealing times of 2.25, 3.5, and 4.9 hours, respectively. After each annealing step the excess losses for TE and TM have been measured using a $\lambda = 1.556$ μm DFB-laser as optical source. The excess loss means the overall loss (without coupling) reduced by the propagation loss of Ti waveguides, which had been measured before the fabrication of the polarizers. No temperature dependence of the TE losses has been found. The TE- and TM-excess losses for each g and after each annealing step are shown in Fig. 16. The data points are the mean values of the six polarizers each, calculated in dB. The standard deviations of the excess losses from the mean values, represented as error bars, are quite high. The main reason is that the alignment of the polarizers relative to the optical waveguide centers could be performed with a limited precision of a few tenth μm only. It can be clearly seen that both the TE- and TM-excess losses increase with enlargement of the annealing time and reduction of g. The polarizers with $g = 10.7$ μm after 3.5 h annealing have the best performance. 26 dB excess loss for the TE-mode has

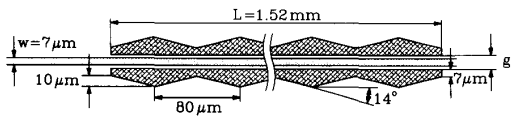

Fig. 15. Detailed design of the TM-pass polarizer.

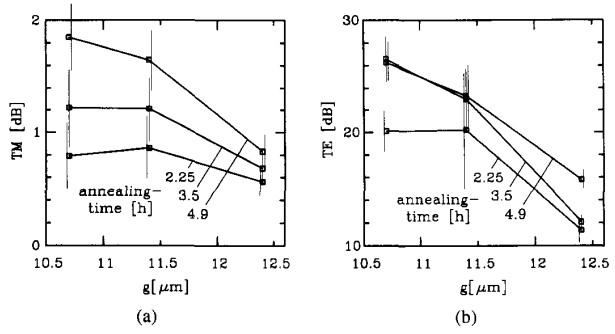

Fig. 16. Measured excess losses for (a) TM and (b) TE versus g after 3 annealing steps.

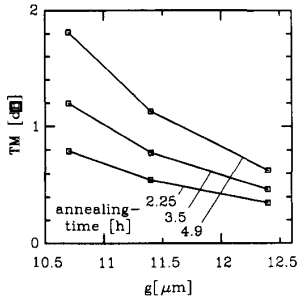

Fig. 17. Calculated results of TM-excess losses versus g for three different annealing times using the BPM.

been obtained, whereas the excess loss for the TM-mode is only 1.2 dB. These results show that a continuous coupling of the supermodes to radiation modes has been achieved, which is equivalent to the prevention of any reflections at the outer polarizer boundaries in the ray optical view.

VI. Discussion and Conclusion

For comparison of experimental and numerical results, the calculated excess losses of the TM-field are shown in Fig. 17. As expected, the attenuation decreases with increasing gap and decreasing annealing time. The calculated excess losses are always lower than the corresponding measured values. For example at a gap of $g = 12.4$ μm the experimental data are between 0.55 dB and 0.85 dB for the various annealing times whereas from the BPM calculations losses of 0.35 dB to 0.65 dB are predicted. The maximum difference of about 0.5 dB occurs for a gap of $g = 11.4$ μm and 4.9 h annealing time.

From the BPM calculation the TE-polarized power in the fundamental mode should be attenuated by more than 25 dB for all cases. In the experiment, however, we found that the attenuation especially for $g = 12.4$ μm is only in the range of 11 to 16 dB. For the narrower gaps it is always above 20 dB. That means, the modelling leads to a stronger attenuation than observed in the experiment. This discrepancy is not fully understood. We attribute most of it to the limited precision of the photolithography. On the other hand, further structural investigations of the proton exchange might be necessary in order to refine the model of the refractive index profile. Although the differences are relatively high, the results show that the tendency of the parameter dependence is sufficiently well described by our theoretical model. This agreement can also be seen from the experimentally observed temperature dependence of the output power dicussed in Section V. Because temperature tuning results in variations of the optical path length within the polarizer, the corresponding changes of the output power is equivalent to the rapidly varying power as a function of the propagation distance evaluated by the BPM calculations (Figs. 8–10).

The width of the gap between the proton exchanged regions determines very critical the polarizer performance. By narrowing the gap the extinction ratio increases, but a higher excess loss for TM-polarized waves occurs as well. The origin of this higher loss is that the TM mode is only weakly guided (or even below cutoff) and its field distribution broadens. For optimum polarizer performance a compromise between acceptable excess loss and extinction ratio must be chosen.

In conclusion, it has been shown that small size integrated optical TM-pass polarizers for wavelengths around $\lambda = 1.5$ μm can be realised in X-cut Y-propagating $LiNbO_3$ by using proton exchanged regions near the Ti-diffused optical waveguide. It has been demonstrated that reflections on the outer boundaries and a subsequent coupling back into the waveguide can result in a small extinction ratio only. Therefore, the outer boundaries had to be modified to prevent such reflections. With zig-zag shaped outer boundaries high extinction ratios and nearly temperature independent operation have been achieved.

By optimizing these critical parameters and with a careful control of all fabrication parameters, polarizers with more than 25 dB extinction ratio and an excess loss of only 1.2 dB for TM-polarized waves have been fabricated.

References

[1] M. Papuchon and S. Vatoux, "Integrated optical polarizer on $LiNbO_3$:Ti channel waveguides using proton exchange," *Electron. Lett.*, vol. 19, pp. 612–613, 1983.

[2] D. A. Smith, J. J. Johnson, K. W. Cheung, J. L. Jackel and J. E. Baran, "Fully integrated two-stage accousto-optic filter with no doppler shift," in *Tech. Dig. Integrated Photon. Res.*, 1990, Opt. Soc. of America, Washington D.C., vol. 5, p. 164, 1990.

[3] H. Herrmann, P. Müller-Reich, V. Reimann, R. Ricken, H. Seibert and W. Sohler, "Integrated optical, TE- and TM-pass, acoustically tunable, double-stage wavelength filters in $LiNbO_3$," *Electron. Lett.*, vol. 28, pp. 642–643, 1992.

[4] L. B. Aronson, G. Rankin, W. R. Trutna and D. W. Dolfi, "Reduced sidelobe integrated acousto-optic filter with birefringence apodization," *Opt. Lett.*, vol. 18, pp. 1721–1723, 1993.

[5] F. Tian, Ch. Harizi, H. Herrmann, V. Reimann, R. Ricken, U. Rust, W. Sohler, F. Wehrmann and S. Westenhöfer, "Polarization independent integrated optical, acoustically tunable double stage wavelength filter in $LiNbO_3$," *J. Lightwave Technol.*, vol. 12, pp. 1192–1197, 1994.

[6] F. Laurell, J. Webjörn, G. Arvidsson, and J. Holmberg, "Wet etching of proton-exchanged lithium niobate—A novel processing technique," *J. Lightwave Technol.*, vol. 10, pp. 1606–1609, 1992.

[7] M. Mc Wright Howerton, W. K. Burns, P. R. Skeath and A. S. Greenblatt, "Dependence of refractive index on hydrogen concentration

in proton exchanged $LiNbO_3$," *IEEE J. Quantum Electron.*, vol. 27, pp. 593–601, 1991.
[8] S. T. Vohra, A. R. Mickelson and S. E. Asher, "Diffusion characteristics and waveguiding properties of proton-exchanged and annealed $LiNbO_3$ channel waveguides," *J. Appl. Phys.*, vol. 66, pp. 5161–5174, 1989.
[9] M. Koshiba, K. Hayata and M. Suzuki, "Approximate scalar finite-element analysis of anisotropic waveguides with off-diagonal elements in a permitivity tensor," *IEEE Trans. Microwave Theory Tech.*, vol. MTT-32, pp. 587–593, 1984.
[10] E. Strake, G. P. Bava, and I. Montrosset, "Guided modes of Ti:$LiNbO_3$ channel waveguides," *J. Lightwave Technol.*, vol. 6, pp. 1126–1134, 1988.
[11] M. D. Feit and J. A. Fleck Jr., "Calculations of dispersion in graded-index multimode fibers by a propagating beam-method," *Appl. Opt.*, vol. 18, pp. 2843–2851, 1979.
[12] N. Mabaya, P. E. Lagasse, and P. Vandenbulcke, "Finite-element analysis of optical waveguides," *IEEE Trans. Microwave Theory Tech.*, vol. MTT-29, pp. 600–605, 1981.
[13] L. Bersiner, U. Hempelmann, and E. Strake, "Numerical analysis of passive integrated-optical polarization splitters: Comparison of finite-element method and beam-propagation method results," *J. Opt. Soc. Am. B.*, vol. 8, pp. 422–433, 1991.
[14] W. Charczenko, I. Januar, and A. R. Mickelson, "Modelling of proton-exchanged and annealed channel waveguides and directional couplers," *J. Appl. Phys.*, vol. 73, pp. 3139–3148, 1993.
[15] J. E. Baran and D. A. Smith, "Adiabatic 2 × 2 polarization splitter on $LiNbO_3$," *IEEE Photon. Technol. Lett.*, vol. 4, pp. 39–40, 1992.

Uwe Hempelmann (M'92) was born in Herford, Germany, in 1962. He received the diploma degree in electrical engineering from the University of Paderborn in 1989.

Since then he has been with the Department of Electromagnetic Theory at the same University, where he is engaged in the numerical analysis of linear and nonlinear integrated optical devices.

Harald Herrmann was born in Martfeld/Germany in 1958. He received the diploma degree in physics from the University of Hannover in 1984. In 1991 he received the Ph.D. degree (Dr. rer. nat.) with a thesis on nonlinear difference frequency generation in lithium niobate waveguides.

In 1984 he joined the Department of Applied Physics of the University of Paderborn/Germany. There he was engaged in the development of color center lasers and in investigations of nonlinear processes in integrated optical waveguides and new electrooptical and acousto-optical devices. He currently works on integrated acousto-optical devices and their applications in optical communication systems and optical instrumentation.

Dr. Herrmann is a member of the German Physical Society.

Gerd Mrozynski (M'84) was born in Berlin on August 25, 1939. He received the Dipl.-Ing. and Dr.-Ing. degrees from the Technical University of Berlin in 1968 and 1972, respectively.

From 1968 to 1970 he was with the Hahn-Meitner-Institut of Nuclear Science, Berlin and from 1970 to 1975 as a Research and Teaching Assistant engaged in the calculation of electromagnetic fields at the Institute of Electromagnetic Theory at the Technical University of Berlin. From 1975 to 1980 he dealt with the design of service integrated networks with optical transmission at the Heinrich-Hertz-Institut for Communications in Berlin. Since 1980 he is Professor of Electromagnetic Theory at the University of Paderborn, Germany. His current interests are in the area of electromagnetic theory and include transmission lines and integrated optics.

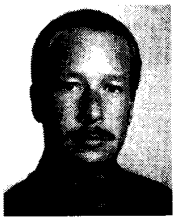

Volker Reimann was born in Olsberg/Germany in 1964. He received the diploma degree in physics from the University of Paderborn/Germany in 1991.

Since 1991 he has been working in the Department of Applied Physics of the University of Paderborn especially on proton exchanged devices in lithium niobate.

Wolfgang Sohler was born in Wangen/Allgäu, Germany, in 1945. He received the Diplom-Physiker and Dr. rer. nat. degrees in physics from the University of Munich/Germany in 1970 and 1974, respectively.

From 1975 to 1980 he was with the University of Dortmund/Germany working on integrated optics. In 1980 he joined the Fraunhofer Institut für Physikalische Metechnik, Freiburg/Germany, as head of the Department of Fiber Optics. Since 1982 he is with the University of Paderborn/Germany as Professor of Applied Physics. His research interests include integrated optics, fiber optics and laser physics. He is the (co-)author of more than 100 journal contributions and of several book chapters. He has been a member of the program committee of several (international) conferences on integrated optics.

Dr. Sohler is a member of the German Physical Society and of the German Society of Applied Optics.